JREE: Vol. 10, No. 4, (Autumn 2023) 22-34

Journal of Renewable Energy and Environment

Journal Homepage: www.jree.ir

Materials and Energy Research Center

MERC

Research Article

An Improved Hottel-Whiller-Bliss Equation for the Nth Photo-Voltaic Thermal-Thermo-Electric Cooler Air Collectors Connected in Series: Exergy Analysis

Gopal Nath Tiwari [a], Prashant Bhardwaj [b*], Sujata Nayak [c]

[a] *BERS Pubic School, Margupur, P. O. Box: 221701, Chilkhar, Ballia (UP), India*
[b] *Department of Mechanical Engineering, Manav Rachna University, P. O. Box: 121004, Faridabad, Haryana, India*
[c] *Legato Health Technologies, P. O. Box: 560045, Bengaluru, Karnataka, India*

PAPER INFO

Paper history:
Received: 26 December 2022
Revised: 10 March 2023
Accepted: 11 March 2023

Keywords:
Photovoltaic Thermal (PVT),
Solar Energy,
Thermo-Electric Cooler (TEC)

ABSTRACT

This study considers N-photovoltaic thermal-thermo electric cooler (PVT-TEC) air collectors connected in series for thermal and electrical performance. An improved Hottel-Whiller-Bliss (HWB) equation and mass flow rate factor were derived for the nth PVT-TEC air collectors. The derivation is based on energy balance equation for each component of N-photovoltaic thermal-thermo electric cooler (PVT-TEC) air collectors connected in series. Further, thermal energy and electrical energy from PV module and TEC were analyzed based on a given design and climatic parameters along with the overall exergy of the proposed system on the hourly and daily bases. Numerical computations were conducted using MATLAB under Indian climatic conditions. The proposed thermal model is valid for all climatic and weather conditions. Based on the numerical computations carried out, the following conclusions were made:

i. The electrical power of PV module decreased with increase in the number of the n^th PVT-TEC air collectors as the electrical power of TEC increased.

ii. The overall instantaneous exergy efficiency decreased with increase in the number of the n^th PVT-TEC air collectors.

iii. Packing factor of TEC was found to be a very sensitive parameter for optimizing the number of PVT-TEC air collectors to ensure maximum overall exergy, and it was found to be β_tec=0.5. for N=7

https://doi.org/10.30501/jree.2023.376480.1516

1. INTRODUCTION

Solar energy is freely available, economical, environmentally-friendly, and sustainable source of energy and it find various applications in our daily lives. The analysis of a solar energy-based system basically depends on the operating temperature. One of the solar energy systems is the thermal system that operates in the medium temperature range (0°C<T<100°C). In this temperature range, a conventional flat plate water/air collector is used for water and air heating. The thermal analysis of conventional Flat Plate Collectors (FPC) has been carried out based on the first law of thermodynamics (energy conservation). The FPC enjoys better performance in the forced mode of operation and requires electrical power. To make FPC self-sustainable, the glass cover is replaced with a photovoltaic (PV) module, which is known as a photovoltaic thermal (PVT) collector (Tiwari et al., 2016; Tiwari & Dubey S., 2010). The PVT collector provides thermal (low-grade energy) and electrical power (high-grade energy). Hence, in order to analyze the PVT collector in the medium temperature range, it is important to consider both the thermal exergy and electrical energy concepts based on the second law of thermodynamics. The combination of both gives the overall exergy of the PVT collector. The exergy analysis is an efficient tool for energy policy-making in terms of quantity and quality of the energy sources including destruction unlike energy (Dincer, 2002; Dincer & Rosen, 2013). Hoseinzadeh et al. carried out exergoeconomic analysis and optimization of reverse osmosis (RO) desalination integrated with geothermal energy (Hoseinzadeh, Yargholi, et al., 2020). The study resulted in a reduction of the total cost rate by 10%. The multi-effect desalination (MED) system was also analyzed by Kariman et al. with negligible exergy destruction (Kariman et al., 2020). Kariman et al. conducted energetic and exergetic analyses of an evaporation desalination system integrated with mechanical vapor recompression circulation (Kariman et al., 2019). They found that the highest exergy destruction occurred in the boiler compartment. Recently, Hoseinzadeh et al. have conducted energy, exergy, and environmental (3E) analyses and optimization of a Coal-Fired 400 MW Thermal Power and micro hydro systems for hot climatic conditions (Hoseinzadeh, Ghasemi, et al., 2020; Hoseinzadeh & Heyns, 2020). Jafari et al. conducted an energy, exergy, and environmental (3E) optimal location assessment of flat-plate collectors for

*Corresponding Author's Email: prashant@mru.edu.in (P. Bhardwaj)
URL: https://www.jree.ir/article_170019.html

Please cite this article as: Tiwari, G. N., Bhardwaj, P., & Nayak, S. (2023). An Improved Hottel-Whiller-Bliss Equation for the Nth Photo-Voltaic Thermal-Thermo-Electric Cooler Air Collectors Connected in Series: Exergy Analysis, *Journal of Renewable Energy and Environment (JREE)*, 10(4), 22-34. https://doi.org/10.30501/jree.2023.376480.1516.

domestic hot water applications in Iran (Jafari et al., 2022).

The classifications of flat plate collectors are summarized as follows:

Conventional flat plate liquid collectors (FPC) operate by transmitting solar energy through a glazed surface, which is then absorbed by a blackened surface to heat the working fluid beneath it (Badiei et al., 2020; Duffie & Beckman W. A., 2013; Sarwar et al., 2020). This method provides only thermal energy and requires grid power for forced mode operation, which enhances its performance.

Photo-voltaic thermal (PVT) liquid collectors: In PVT collector, the glass of flat plate collector (FPC) is replaced by photovoltaic (PV) module. It gives both thermal and electrical energy to become self-sustained. It also operates in the medium range of temperatures (Arslan et al., 2020; Chow, 2010; Dupeyrat et al., 2014; Hocine et al., 2015; Tiwari & Dubey S., 2010; Zondag et al., 2003).

PVT-CPC collectors: When a compound parabolic concentrator (CPC) is integrated on top of a photovoltaic thermal (PVT) collector, the resulting system is called a PVT-CPC. This configuration allows for a more concentrated solar energy, resulting in more thermal energy production but lower electrical power output due to the high operating temperature. Additionally, PVT-CPC systems are self-sustained and can operate at higher temperatures compared to traditional PVT collectors (Atheaya et al., 2016; Cabral et al., 2019; Kostić et al., 2010; Proell et al., 2017; Tiwari et al., 2018).

PVT-TEC collectors: In this case, the thermo-electric cooler (TEC) is attached to the back of the absorber of PVT collector. In addition to PV module, TEC generates for additional electric power in addition to PV module due to Peltier effect with temperature difference. It is efficient and operates at medium temperature range (Dimri et al., 2018; Huen & Daoud, 2017; Ong et al., 2017; Sudharshan et al., 2016; Yin et al., 2017; Zhang et al., 2014; Zhu et al., 2016).

In all the cases mentioned above, the single collector was used. Furthermore, to increase both thermal energy and electrical energy, various researchers have analyzed the following combinations :

All PVT collectors were connected in series: Increasing the number of PVT collectors results in higher thermal output but lower electrical power output from the PV module due to the high temperature of the solar cell (Dubey & Tiwari, 2008; Li et al., 2020; Ma et al., 2020; Shyam et al., 2016; Tiwari et al., 2018).

Series and parallel separately: The operating temperature in the parallel configuration is lower than that in the series connection for a given total number of PVT collectors. Therefore, parallel connection is considered more efficient than series connection in this case (Kotb et al., 2019; Sharaf & Orhan, 2018; Vega & Cuevas, 2020).

The electrical efficiency of the solar cell in PVT-TEC air collectors is highly sensitive to the operating temperature (Evans, 1981; Skoplaki & Palyvos, 2009). When PVT air collectors are connected in series, the operating temperature of the PVT collector increases with an increase in the number of collectors. As a result, the electrical efficiency of the solar cell in the PVT collector decreases while the electrical efficiency of the TEC increases. However, this effect has not been considered for N-PVT-TEC collectors that are connected in series.

In this connection, we considered N-PVT-TEC air collectors connected in only series to evaluate the overall exergy of the PVT-TEC system which, to the best of our knowledge, has not been done before. Further, we derived an inproved Hottel-Wills- Beckman (HWB) equation and calculated the overall hourly exergy and exergy efficiency of the proposed system. The proposed system was evaluated based on the varying numbers of PVT-TEC collectors from n=1 to N. Additionally, we investigated the effect of the correction factor (CF) on the mass flow rate factor (F_(R,n^th)) .

2. WORKING PRINCIPLE OF OPAQUE PV-TEC AIR COLLECTOR

In the present case, we considered fully covering an opaque PV module with an air duct below it. The thermo-electrical cooler (TEC) module is attached to the base of PV module with packing factor (β_tec<1) less than one, as shown in Fig. 1a and suggested in (Sudharshan et al., 2016). By using the Eq. 1, the packing factor of TEC can be calculated.

$$\beta_{\text{tec}} = \frac{\text{Number of TEC cell area} \times \text{area of one TECcell}}{\text{Area of opaque PV modul}} \leq 1 \qquad (1)$$

In order to remove thermal energy from the bottom end of PV and TEC modules, the working fluid was considered as air and allowed to flow through an air duct. As a result, flowing air is heated and the bottom of TEC is cooled, giving rise a temperature difference across TEC that provides electrical current due to Peltier effect, as mentioned earlier. Therefore, the total electric power of PVT-TEC is the sum of electrical power generated from PV module and TEC. The schematic illustration of the opaque PV-TEC collector with air duct is shown in Fig. 1(a). To increase the temperature, the outlet of the first PVT-TEC air collector is connected to the inlet of the second collector, as shown in Fig.1b. This process continues until the Nth PVT-TEC air collector is reached. The number of PVT-TEC air collectors that can be connected in series depends significantly on the mass flow rate (0.025-0.25 kg/s) required to achieve the desired outlet air temperature. The design parameters of the PVT-TEC air collector are given in Table 1.

According to Fig. 1a, part of solar radiation is absorbed by solar cell of PV module $[\tau_g \alpha_{sc} I(t) bdx]$ after transmission through glass cover. Following the process of absorption, the solar cell of opaque PV module converts into electrical energy $[\eta_{sc} \tau_g I(t) bdx]$ depending upon its electrical efficiency (η_{sc}). Further, some portion of the absorbed radiation is directly transferred to ambient air through the top glass cover of the opaque PV module $[U_t(T_{sc} - T_a) bdx]$ and the remaining is indirectly transferred to the air flowing below the TEC $[U_{b,ca}(T_{sc} - T_f)(1 - \beta_{tec}) bdx]$. Moreover, thermal energy is transferred from the back of solar cells to the top of TEC $[h_t(T_{sc} - T_{tec,top})\beta_{tec} bdx]$ through the packing area of the TEC. The thermal circuit diagram of the PVT-TEC air collector is shown in Figure. 1c.

Table 1. Design parameters of the PVT-TEC air collector (Dimri et al., 2018)

A_m	0.1332 m^2	K_{tec}	1.82 W/mK
b	0.36 m	L_{tec}	0.004 m
L	0.37 m	K_i	0.166 W/mK
L_f	0.01 m	L_i	0.100 m
α_{sc}	0.9	K_f	0.02622 W/mK
τ_g	0.95	h_{tf}	2.21 W/m^2K
η_o	0.15	U_b	0.62 W/m^2K
η_{tec}	0.08	U_{tec}	435.2 W/m^2K
β_o	0.0045/K	$U_{tec,top-a}$	4.2118 W/m^2K
c_f	1005 J/kgK	$U_{tec,bottom-a}$	4.1714 W/m^2K
$\dot{m}_f$	0.003 kg/s	U_{fa}	2.3095 W/m^2K
R_c	10^{-4} m^2 K/W	h_{p1}	0.3618
K_g	0.816 W/mK	h_{p2}	0.9904
L_g	0.003 m	h_{p3}	0.6018
K_t	0.033 W/mK	$(\alpha\tau)_{eff}$	0.7225
L_t	0.005 m	$(\alpha\tau)'_{eff}$	0.2382

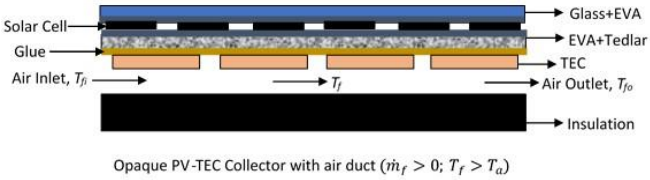

Figure 1a. Cross-sectional view of the single PVT-TEC air collector

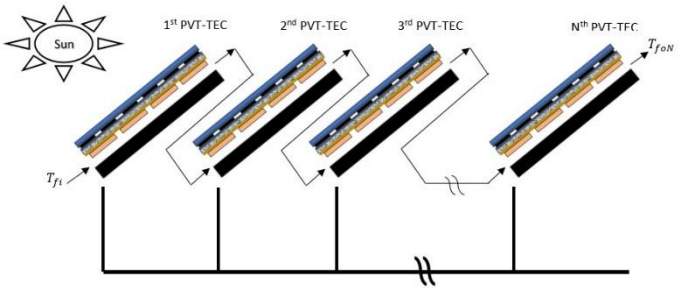

Figure 1b. The N-PVT-TEC air collectors connected in series

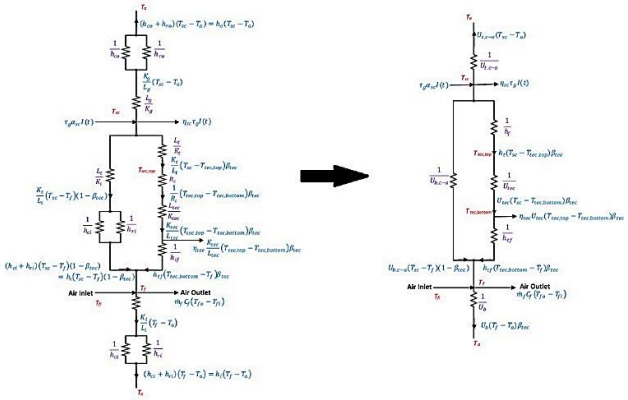

Figure 1c. Thermal circuit diagram of the PVT-TEC air collector (Sudharshan et al., 2016)

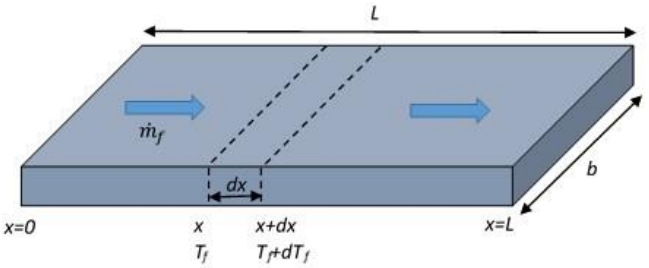

Figure 2. An elemental area of 'bdx' for flowing air below air duct

3. THERMAL MODELING

The following assumptions are made for thermal modeling:

(i) The proposed system is in a quasi-steady state
(ii) Thermal heat capacity of each component is neglected
(iii) No temperature stratification along thickness of each component is needed.
(iv) The flow of air is in a stream line.
(v) Design parameters and area $(A_m)$of each PVT-TEC air collectors are the same.

3.1 Energy Balance of PVT-TEC Air Collector (Dimri et al., 2018)

(a) Solar cell of the opaque PV module

$$\tau_g\alpha_{sc}I(t)bdx = U_{t,c-a}(T_{sc}-T_a)bdx + h_t(T_{sc}-T_{tec,top})\beta_{tec}bdx + U_{b,c-a}(T_{sc}-T_f)(1-\beta_{tec})bdx + \eta_{sc}\tau_g I(t)bdx \quad \ldots(2)$$

where

$$\beta_{tec} = \frac{NumberofTECmodules \times AreaofoneTECmodule}{AreaofPVmodule/collector}$$

(b) For tedlar:

$$h_t(T_{sc}-T_{tec,top})\beta_{tec}bdx = U_{tec}(T_{tec,top}-T_{tec,bottom})\beta_{tec}bdx \quad \ldots(3)$$

(c) For TEC module:

$$U_{tec}(T_{tec,top}-T_{tec,bottom})\beta_{tec}bdx = h_{tf}(T_{tec,bottom}-T_f)\beta_{tec}bdx + \eta_{tec}U_{tec}(T_{tec,top}-T_{tec,bottom})\beta_{tec}bdx \quad \ldots(4)$$

where U_{tec} is the overall heat transfer coefficient between TEC module and tedlar (Figure 1a). The numerical value of U_{tec} is calculated as:

$$U_{tec} = \left[R_c + \frac{L_{tec}}{K_{tec}}\right]^{-1} \quad \ldots(5)$$

where R_c is the thermal contact resistance at thermoelectric leg-electrode interfaces. The literature reports a range of thermal contact resistance levels that fall within $1 \times 10^{-6} - 5 \times 10^{-4}$ m^2Kelvin/W (Zhang et al., 2014). Thermal contact resistance (R_c) is chosen to be 10^{-4} m^2Kelvin/W in the current study.

(d) For air flowing below TEC module (Figure 2):

As mentioned above, the air flowing through the air duct received the rate of thermal energy $[h_{tf}(T_{tec,bottom} - T_f)\beta_{tec}bdx]$and $[U_{b,c-a}(T_{sc} - T_f)(1-\beta_{tec})bdx]$ and the energy balance can be written for the flowing air as follows:

$$h_{tf}(T_{tec,bottom} - T_f)\beta_{tec}bdx + U_{b,c-a}(T_{sc} - T_f)(1-\beta_{tec})bdx = \dot{m}_f c_f \frac{dT_f}{dx}dx + U_b(T_f - T_a)bdx \quad \ldots(6)$$

3.2 Analytical Expression for an Outlet Fluid Temperature of N-PVT-TEC Air Collector

By adopting the thermal mode proposed by various researchers (Dimri et al., 2018; Tiwari et al., 2016; Tiwari & Dubey S., 2010), an expression for solar cell temperature (T_{sc}), TEC top ($T_{tec,top}$), and TEC bottom ($T_{tec,bottom}$) temperatures can be obtained via the elimination process in Eqs. 1-4 as follows:

$$T_{sc} = \frac{(\alpha\tau)_{eff}I(t) + U_{t,c-a}T_a + U_{b,c-a}(1-\beta_{tec})T_f + h_t\beta_{tec}T_{tec,top}}{U_{t,c-a} + U_{b,c-a}(1-\beta_{tec}) + h_t\beta_{tec}} \quad \ldots(7)$$

$$T_{tec,top} = \frac{h_{p1}(\alpha\tau)_{eff}I(t) + U_{tec,top-a}T_a + U_{tec,top-f}T_f + U_{tec}\beta_{tec}T_{tec,bottom}}{U_{tec,top-a} + U_{tec,top-f} + U_{tec}\beta_{tec}} \quad \ldots(8)$$

$$T_{tec,bottom} = \frac{(\alpha\tau)'_{eff}I(t) + (1-\eta_{tec})U_{tec,bottom-a}T_a + [(1-\eta_{tec})U_{tec,bottom-f} + h_{tf}\beta_{tec}]T_f}{(1-\eta_{tec})U_{tec,bottom-a} + (1-\eta_{tec})U_{tec,bottom-f} + h_{tf}\beta_{tec}} \quad \ldots(9)$$

The expressions for $(\alpha\tau)_{eff}$, $(\alpha\tau)'_{eff}$, h_t, h_{p1}, h_{tf}, $U_{t,c-a}$, $U_{b,c-a}$, $U_{tec,top-a}$, $U_{tec,top-f}$, $U_{tec,bottom-a}$, and $U_{tec,bottom-f}$ are given in Appendix A (Dimri et al., 2018).

By using Eqs. (7) – (9), Eq. (6) can be rewritten as follows:

$$\frac{dT_f}{dx} + aT_f = f(t) \quad \ldots(10)$$

where

$a = \frac{(U_{fa}+U_b)b}{\dot{m}_f c_f}$, $f(t) = \frac{(\alpha\tau)_{m-eff}bI(t)+U_{Lm}bT_a}{\dot{m}_f c_f}$;

$\frac{f(t)}{a} = \frac{(\alpha\tau)_{m-eff}I(t)+(U_{fa}+U_b)T_a}{(U_{fa}+U_b)} = \left[\frac{(\alpha\tau)_{m-eff}}{U_{Lm}}I(t) + T_a\right]$

$(\alpha\tau)_{m-eff} = [h_{p3}(\alpha\tau)'_{eff} + h'_{p1}(\alpha\tau)_{eff} + h'_{p2}h_{p1}(\alpha\tau)_{eff} + h'_{p3}(\alpha\tau)'_{eff}]$ and $U_{Lm} = (U_{fa} + U_b)$

The expressions ofU_{fa}, U_b, h_{p3}, h'_{p1}, h'_{p2} and $h'_{p3}$are defined in Appendix A (Dimri et al., 2018)

The solution of Eq. 8 can be obtained through the initial condition, $i.e.,\ T_f|_{x=0} = T_{fi}$ (Dimri et al., 2018). The solution to Eq. (10) is as follows:

$$T_f = \left[\frac{(\alpha\tau)_{m-eff}}{U_{Lm}}I(t) + T_a\right](1 - e^{-ax}) + T_{fi}e^{-ax} \quad \ldots(11)$$

By using [Eq.11] and at x= $i.e.T_f|_{x=L} = T_{fo1}$, the fluid temperature at outlet (T_{fo1}) of the first PVT-TEC air collector can be calculated as

$$T_{fo1} = \left[\frac{(\alpha\tau)_{m-eff}}{U_{Lm}}I(t) + T_a\right]\left(1 - e^{-\frac{U_{Lm}A_m}{\dot{m}_f c_f}}\right) + T_{fi}e^{-\frac{U_{Lm}A_m}{\dot{m}_f c_f}} \quad \ldots(12)$$

The above equation is also derived from the referenced study (Dimri et al., 2018).

If an outlet of the first PVT-TEC air collector, T_{fo1} [Eq. 12], is connected to the inlet of the second PVT-TEC air collector, T_{fi2}, Figure 1b, then the expression of the outlet of the 2nd PVT-TEC will be as follows:

$$T_{fo2} = \left[\frac{(\alpha\tau)_{m-eff}}{U_{Lm}}I(t) + T_a\right]\left(1 - e^{-\frac{U_{Lm}A_m}{\dot{m}_f c_f}}\right) + T_{fo1}e^{-\frac{U_{Lm}A_m}{\dot{m}_f c_f}} \quad \ldots(13)$$

After substituting T_{fo1} from Eq. 12 into Eq. 13, we get:

$$T_{fo2} = \left[\frac{(\alpha\tau)_{m-eff}}{U_{Lm}}I(t) + T_a\right]\left(1 - e^{-\frac{2U_{Lm}A_m}{\dot{m}_f c_f}}\right) + T_{fi}e^{-\frac{2U_{Lm}A_m}{\dot{m}_f c_f}} \quad \ldots(14)$$

Now, the outlet of the second PVT-TEC air collector, T_{fo2}, will be the inlet of the third PVT-TEC air collector for series connection. Then, we have:

$$T_{fo3} = \left[\frac{(\alpha\tau)_{m-eff}}{U_{Lm}}I(t) + T_a\right]\left(1 - e^{-\frac{2U_{Lm}A_m}{\dot{m}_f c_f}}\right) + T_{fo2}e^{-\frac{2U_{Lm}A_m}{\dot{m}_f c_f}} \quad \ldots(15)$$

Upon solving Eq.15 as mentioned above, one gets:

$$T_{fo3} = \left[\frac{(\alpha\tau)_{m-eff}}{U_{Lm}}I(t) + T_a\right]\left(1 - e^{-\frac{3U_{Lm}A_m}{\dot{m}_f c_f}}\right) + T_{fi}e^{-\frac{3U_{Lm}A_m}{\dot{m}_f c_f}} \quad \ldots(16)$$

Similarly, for N-PVT-TEC air collectors connected in series, an expression for an outlet air temperature at the end of N-PVT-TEC air collector T_{foN} can be written as follows:

$$T_{foN} = \left[\frac{(\alpha\tau)_{m-eff}}{U_{Lm}} I(t) + T_a\right]\left(1 - e^{-\frac{NU_{Lm}A_m}{\dot{m}_f c_f}}\right) + T_{fi} e^{-\frac{NU_{Lm}A_m}{\dot{m}_f c_f}} \quad \ldots (17a)$$

The above equation is a new expression for N-PVT-TEC air collectors connected in series.

3.3 Improved Hottel-Whillier-Bliss (HWB) Equation

The rate of thermal energy at the n[th] PVT-TEC air collector will be as follows:

$$\dot{Q}_{uth,n^{th}} = \dot{m}_f C_f \left(T_{fon} - T_{fon-1}\right)$$

Substituting T_{fon} and T_{fon-1} from Eq. 17a in terms of T_{fi} into the above equation, we get:

$$\dot{Q}_{uth,n^{th}} = \dot{m}_f C_f \left\{\left[\frac{(\alpha\tau)_{m-eff}}{U_{Lm}} I(t) + T_a\right]\left(1 - e^{-\frac{nU_{Lm}A_m}{\dot{m}_f c_f}}\right) + T_{fi} e^{-\frac{nU_{Lm}A_m}{\dot{m}_f c_f}}\right\} - \left\{\left[\frac{(\alpha\tau)_{m-eff}}{U_{Lm}} I(t) + T_a\right]\left(1 - e^{-\frac{(n-1)U_{Lm}A_m}{\dot{m}_f c_f}}\right) + T_{fi} e^{-\frac{(n-1)U_{Lm}A_m}{\dot{m}_f c_f}}\right\}$$

$$\dot{Q}_{uth,n^{th}} = \dot{m}_f C_f \left(1 - e^{-\frac{U_{Lm}A_m}{\dot{m}_f c_f}}\right)\left\{\left[\frac{(\alpha\tau)_{m-eff}}{U_{Lm}} I(t) + T_a\right] - T_{fi}\right\} e^{-\frac{(n-1)U_{Lm}A_m}{\dot{m}_f c_f}}$$

$$\dot{Q}_{uth,n^{th}} = \dot{m}_f C_f \left(1 - e^{-\frac{U_{Lm}A_m}{\dot{m}_f c_f}}\right) CF \left[\frac{(\alpha\tau)_{m-eff}}{U_{Lm}} I(t) - \left(T_{fi} - T_a\right)\right] \quad \ldots (17b)$$

where

$$CF = e^{-\frac{(n-1)U_{Lm}A_m}{\dot{m}_f c_f}} = 1 \; for \; n = 1 \; otherwise < 1 \; for \; n > 1$$

The above equation is valid for $n < N$.

Instantaneous thermal efficiency of the n^{th} PVT-TEC air collector is given by

$$\eta_{i,n^{th}} = \frac{\dot{Q}_{uth,n^{th}}}{I(t)A_m} = \frac{\dot{m}_f C_f}{A_m U_{Lm}}\left(1 - e^{-\frac{U_{Lm}A_m}{\dot{m}_f c_f}}\right) CF \left[(\alpha\tau)_{m-eff} - U_{Lm}\frac{\left(T_{fi} - T_a\right)}{I(t)}\right] \quad \ldots (17c)$$

The above equation is the improved thermal characteristic equation of the n[th] PVT-TEC air collector (improved Hottel-Whillier-Bliss (HWB) equation) that is derived for the first time to be used for indoor testing under standard test conditions (STC). For n=1, Eq. 17c is reduced to the following:

$$\eta_{i,1^{st}} = \frac{\dot{Q}_{uth,n^{th}}}{I(t)A_m} = \frac{\dot{m}_f C_f}{A_m U_{Lm}}\left(1 - e^{-\frac{U_{Lm}A_m}{\dot{m}_f c_f}}\right) \left[(\alpha\tau)_{m-eff} - U_{Lm}\frac{\left(T_{fi} - T_a\right)}{I(t)}\right] \quad \ldots (17d)$$

which is Hottel-Whillier-Bliss (HWB) equation for conventional PVT-TEC air collector.

3.4 Improved Electrical Analysis

Now, an average fluid temperature of the n^{th} PVT-TEC air collector ($n < N$) can be expressed as follows:

$$\bar{T}_{f,n^{th}} = \frac{T_{fon} + T_{fon-1}}{2} \quad \ldots (18)$$

For the first PVT-TEC air collector, $T_{fon-1} = T_{fi}$.

At the known hourly numerical values of $\bar{T}_{f,n^{th}}$, average values of $\bar{T}_{sc}$, $\bar{T}_{tec,top}$, and $\bar{T}_{tec,bottom}$ can be determined using the following equations:

$$\bar{T}_{sc,n^{th}} = \frac{(\alpha\tau)_{eff} I(t) + U_{t,c-a}T_a + U_{b,c-a}(1-\beta_{tec})\bar{T}_{f,n^{th}} + h_t\beta_{tec}T_{tec,top}}{U_{t,c-a} + U_{b,c-a}(1-\beta_{tec}) + h_t\beta_{tec}} \quad \ldots (19)$$

$$\bar{T}_{tec,top,n^{th}} = \frac{h_{p1}(\alpha\tau)_{eff} I(t) + U_{tec,top-a}T_a + U_{tec,top-f}\bar{T}_{f,n^{th}} + U_{tec}\beta_{tec}T_{tec,bottom}}{U_{tec,top-a} + U_{tec,top-f} + U_{tec}\beta_{tec}} \quad \ldots (20)$$

$$\bar{T}_{tec,bottom,n^{th}} = \frac{(\alpha\tau)'_{eff} I(t) + (1-\eta_{tec})U_{tec,bottom-a}T_a + \left[(1-\eta_{tec})U_{tec,bottom-f} + h_{tf}\beta_{tec}\right]\bar{T}_{f,n^{th}}}{(1-\eta_{tec})U_{tec,bottom-a} + (1-\eta_{tec})U_{tec,bottom-f} + h_{tf}\beta_{tec}} \quad \ldots (21)$$

The efficiency of a PV module of the n^{th} PVT-TEC air collector is given as follows (Evans, 1981):

$$\eta_{m,n^{th}} = \tau_g\eta_o\left[1 - \beta_o\left(\bar{T}_{sc,n^{th}} - T_o\right)\right] \quad \ldots (22)$$

where η_o is the efficiency of the PV module at Standard Test Condition (STC), i.e., I(t) = 1000 W/m^2 and To = 25°C, and β_o is the temperature thermal expansion coefficient.

The rate of an electrical energy generated by PV module at the n^{th} PVT-TEC air collector for one packing ($\beta_{sc} = 1$) is given as follows:

$$\dot{E}_{PV,n^{th}} = \eta_{m,n^{th}} I(t) A_m \quad \ldots(23)$$

The rate of thermal energy received from the n^{th} PVT-TEC air collector using the TEC module for the packing area of $(\beta_{tec} A_m)$, i.e., $U_{tec}(\bar{T}_{tec,top,n^{th}} - \bar{T}_{tec,bottom,n^{th}})\beta_{tec} A_m$, when multiplied with η_{tec}, gives an expression for the electrical energy generated by the TEC module as (Dimri et al., 2018):

$$\dot{E}_{\mathrm{TEC,n^{th}}} = \eta_{tec} U_{tec}(\bar{T}_{tec,top,n^{th}} - \bar{T}_{tec,bottom,n^{th}})\beta_{tec} A_m \quad \ldots(24)$$

where η_{tec} is the conversion efficiency from thermal energy into electrical energy of the TEC module.

The total rate of electrical energy ($\dot{E}_{el,n^{th}}$) generated by the n^{th}opaque PV-TEC air collector can be calculated by adding electrical energy generated by PV module, $\dot{E}_{PV,n^{th}}$, according to Eq.15, and the electrical energy generated by the TEC module, $\dot{E}_{\mathrm{TEC,n^{th}}}$, according to Eq.17.

$$\dot{E}_{el,n^{th}} = \dot{E}_{PV,n^{th}} + \dot{E}_{TEC,n^{th}} \quad \ldots(25a)$$

The improved total rate of electrical energy, $\dot{E}_{e-N}$, generated by the n-opaque PV-TEC air collector can be evaluated as

$$\dot{E}_{el-N} = \sum_{i=1}^{N} \dot{E}_{eli,n^{th}} \quad \ldots(25b)$$

The overall instantaneous total electrical efficiency of the n^{th} opaque PV-TEC air collector can be obtained as follows:

$$\eta_{i,el,n^{th}} = \frac{\dot{E}_{el,n^{th}}}{A_m I(t)} \quad \ldots(26)$$

3.5 Overall Instantaneous Thermal Efficiency

The rate of useful thermal energy gained from the N-opaque PV-TEC air collector is calculated as follows:

$$\dot{Q}_{u,th-N} = \dot{m}_f c_f (T_{foN} - T_{fi}) \quad \ldots(27a)$$

Substituting $T_{foN}$from Eq. 17a into Eq. 27a, we get:

$$\dot{Q}_{u,th-N} = \dot{m}_f c_f \left(1 - e^{-\frac{NU_{Lm}A_m}{\dot{m}_f c_f}}\right)\left[\frac{(\alpha\tau)_{m-eff}}{U_{Lm}} I(t) - (T_{fi} - T_a)\right] \quad \ldots(27b)$$

Further, the overall instantaneous thermal efficiency, $\eta_{i,th-N}$, is defined as follows:

$$\eta_{i,th-N} = \frac{\dot{Q}_{u,th-N}}{NA_m I(t)} = \frac{\dot{m}_f c_f}{NA_m}\left(1 - e^{-\frac{NU_{Lm}A_m}{\dot{m}_f c_f}}\right)\left[\frac{(\alpha\tau)_{m-eff}}{U_{Lm}} - \frac{(T_{fi} - T_a)}{I(t)}\right]$$

or,

$$\eta_{i,th-N} = F_{RN}\left[(\alpha\tau)_{m-eff} - U_{Lm}\frac{(T_{fi} - T_a)}{I(t)}\right] \quad \ldots(27c)$$

where

$$F_{RN} = \frac{\dot{m}_f c_f}{NA_m U_{Lm}}\left(1 - e^{-\frac{NU_{Lm}A_m}{\dot{m}_f c_f}}\right)$$

Here, N=1 Eq. 27c is exactly the same as Eq. 17d.

Eq. 27c is the improved characteristic equation for the N-PVT_TEC air collector, derived for the first time, and it is similar to those derived by Hottel-Whillier-Bliss (HWB) for the flat plate collector (Duffie & Beckman W. A., 2013; Tiwari et al., 2016).

With reference to (Bejan, 1978; Cengel & Boles, 2015; Ouyang & Li, 2016), the exergy of hourly thermal energy$\dot{E}x_{u,th-N}$ (high-grade energy) obtained from the N-opaque PV-TEC air collector can be calculated through the following expression:

$$\dot{E}x_{u,th-N} = \dot{m}_f c_f \left[(T_{foN} - T_{fi}) - (T_a + 273) ln\frac{(T_{foN} + 273)}{(T_{fi} + 273)}\right] \quad \ldots(28)$$

From Eqs. 25b and 28, the overall hourly exergy, $\dot{E}x_{ou-N}$ of the N-opaque PV-TEC air collectors is written as:

$$\dot{E}x_{ou-N} = \dot{E}_{el-N} + \dot{E}x_{u,th-N} \quad \ldots(29)$$

The overall hourly instantaneous exergy efficiency,$\eta_{i,ov-ex}$,$\dot{E}x_{ou}$ of N-opaque PV-TEC air collectors is written as:

$$\eta_{i,ov-ex-N} = \frac{\dot{E}x_{ou-N}}{NA_M I(t)} \quad \ldots(30)$$

Here, N varies from 1 to N=12

Of note, the packing factor of the TEC module is taken as unity ($\beta_{tec} = 1$) in the numerical calculations for the N- opaque PV-TEC air collector.

4 METHODOLOGY FOR NUMERICAL COMPUTATION

The following methodology is developed:

Step 1: The input design and climatic parameters presented in Table 1 and Figure 3 are considered.

Step 2: First, the hourly variation of average fluid ($\bar{T}_{f,n^{th}}$) is determined according to Eq. 18 with help of Eq. 17 and then, the average solar cell ($\bar{T}_{sc,n^{th}}$), TEC top ($\bar{T}_{tec,top,n^{th}}$), and TEC bottom ($\bar{T}_{tec,bottom,n^{th}}$) are calculated using Eq. 19, Eq. 20, and Eq. 21, respectively, at the 12th air collector.

Step 3: Upon determining the hourly variation of average solar cell temperature ($\bar{T}_{sc}$), as outlined in Step 2, electrical

efficiency ($\eta_{i,el,n^{th}}$) at 1st, 3rd, 5th, 7th, 9th, and 12th PVT-TEC air collectors is evaluated.

Step 4: After determining average solar cell($\bar{T}_{sc,n^{th}}$)using Eq. 19, TEC top($\bar{T}_{tec,top,n^{th}}$) using Eq. 20, and TEC bottom($\bar{T}_{tec,bottom,n^{th}}$) using Eq.21 at 12th air collector from Step 2, the hourly variations of electrical energy from PV module ($\dot{E}_{PV,n^{th}}$) using Eq. 23 and TEC ($\dot{E}_{TEC,n^{th}}$) using Eq. 24 at 1st, 3rd, 5th, 7th, 9th, and 12th PVT-TEC air collectors are calculated.

Step 5: Hourly variation of total electrical energy($\dot{E}_{el,n^{th}}$) is calculated using Eq. 25a, which is the sum of electrical energy from PV and TEC, as outlined in Step 4, at the 1st, 3rd, 5th, 7th, 9th, and 12th PVT-TEC air collectors.

Step 6: Eq. 28 is used to compute hourly variation of the overall hourly exergy, $\dot{E}x_{ou}$ of N-opaque PV-TEC air collector at the 1st, 3rd, 5th, 7th, 9th, and 12th PVT-TEC air collectors.

Step 7: Variations of the instantaneous thermal efficiency ($\eta_{i,n^{th}}$) using Eq. 16c and total electrical efficiency ($\eta_{i,el,n^{th}}$) using Eq. 26 with $\frac{(T_{fi}-T_a)}{I(t)}$ are determined at the 1st, 3rd, 5th, 7th, 9th, and 12th PVT-TEC air collectors.

Step 8: Hourly variation of total exergy, Eq. 29 and its efficiency, Eq. 30 for N= 1.3.5.7.9 and 12 are calculated.

Step 9: Finally, the impacts of TEC packing factor β_{tec} (0,0.5 and 1) on the hourly variation of total exergy, Eq. 28, and efficiency, Eq. 30, for N= 7 are evaluated.

Step 10: Results for $T_{tec\text{-}bottom}$ are compared with the experimental findings of Dimri N. et al. (Dimri et al., 2018) to validate the viability of the proposed model, as shown in Figure 12

5 RESULTS AND DISCUSSION

The hourly variation of average fluid(T¯_(f,n^th)), solar cell(T¯_(sc,n^th)), TEC top(T¯_(tec,top,n^th)), and TEC bottom (T¯_(tec,bottom,n^th)) at the 2nd and 12th air collectors for design parameters given in Table 1 and climatic parameters given in Figure 3 are shown in Figure 4. Of note, the average solar cell temperature, T¯_(sc,n^th), is maximum at the 2nd PVT-TEC air collector and minimum at the 12nd PVT-TEC air collector. This indicates that inlet temperature of PVT-TEC in a series connection plays a notable role to determine thermal energy, electrical energy from PV module, and TEC of PVT-TEC air collector. This trend occurs after the 4th PVT-TEC air collector. Such observations have not been yet reported. It is further clear that solar cell temperature is maximum and the bottom of TEC material is minimum at the 12th PVT=TEC air collector (Figure 4b), compared to the 2nd PVT-TEC air collector (Figure 4a). In this case, electrical power from (i) solar cell, which depends only on solar cell temperature [Eq. 22], and (ii) TEC, which depends on difference of top and bottom temperatures, will be produced [Eq. 24]. Further, the temperature of the top surface of TEC is higher than the bottom temperature of TEC, as shown in all the nth PVT-TEC air collectors in Figure 4.

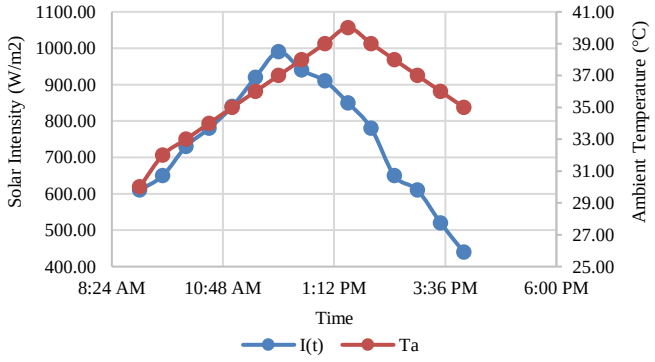

Figure 3. Hourly variation of solar intensity and ambient air temperature for a typical day of summer climatic conditions

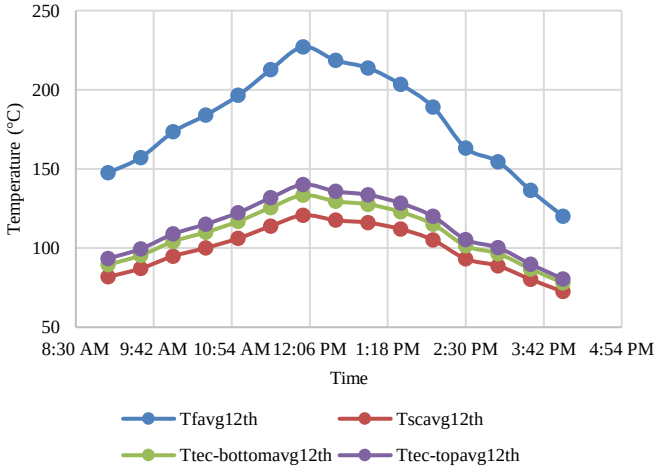

Figure 4a Hourly variation of average fluid($\bar{T}_{f,n^{th}}$) (Eq. 18), solar cell($\bar{T}_{sc,n^{th}}$) (Eq. 19), TEC top($\bar{T}_{tec,top,n^{th}}$) (Eq. 20), and TEC bottom($\bar{T}_{tec,bottom,n^{th}}$) (Eq.19) at the 12th air collector for $n^{th} = 2$ and $n < 4$

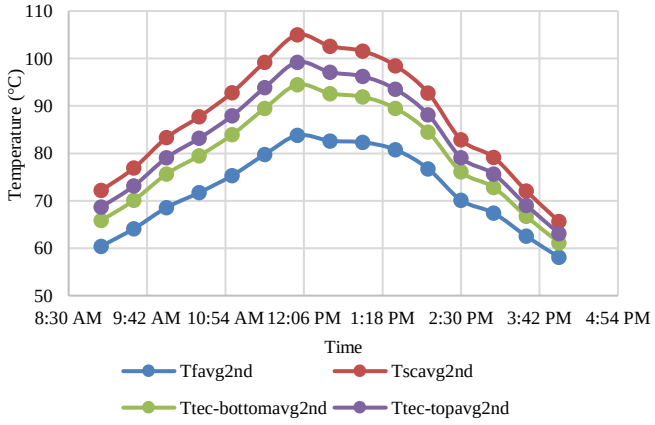

Figure 4b. Hourly variation of average fluid ($\bar{T}_{f,n^{th}}$) (Eq. 18), solar cell ($\bar{T}_{sc,n^{th}}$) (Eq. 19), TEC top ($\bar{T}_{tec,top,n^{th}}$) (Eq. 20), and TEC bottom ($\bar{T}_{tec,bottom,n^{th}}$) (Eq.21) at the 12th air collector

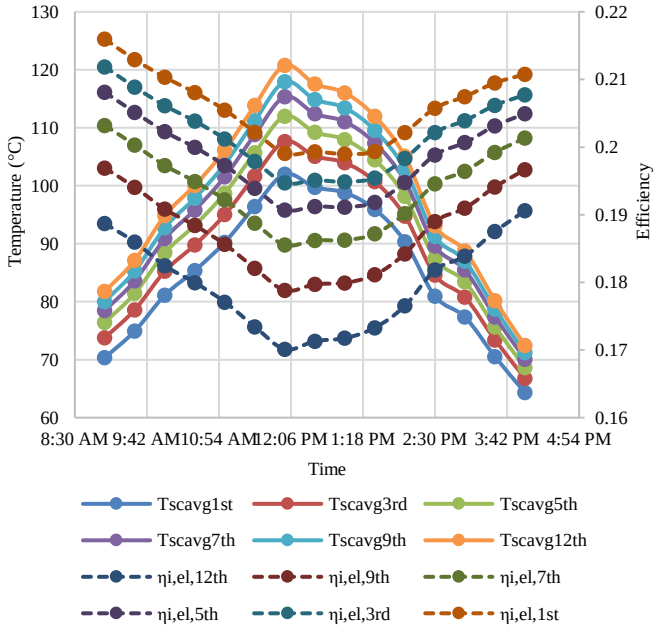

Figure 5. Hourly variation of average solar cell temperature($\bar{T}_{sc,n^{th}}$) ($Eq.19$) and electrical efficiency ($\eta_{i,el,n^{th}}$) (Eq. 22) at the 1st, 3rd, 5th, 7th, 9th, and 12th PVT-TEC air collectors

Figure 5 shows the hourly variation of average solar cell temperature($\bar{T}_{sc,n^{th}}$), Eq. 19, and electrical efficiency ($\eta_{i,el,n^{th}}$), Eq. 22, at the 1st, 3rd, 5th, 7th, 9th and 12th PVT-TEC air collectors. One can infer from Figure 5 that as the value of n in the nth PVT-TEC air collector increases, the average solar cell temperature($\bar{T}_{sc}$) increases, but increment in the average solar cell temperature($\bar{T}_{sc}$) slows down, especially after the 5thPVT-TEC air collector. Further, the electrical efficiency ($\eta_{i,el,n^{th}}$) decreases as the value of n in the nth PVT-TEC air collector increases due to the higher operating temperature per expectation. In this case, the decrement in electrical efficiency ($\eta_{i,el,n^{th}}$) is observed after the 5th PVT-TEC air collector. Therefore, it can be stated that the number of optimum PVT-TEC air collectors is five for design parameters shown in Table 1.

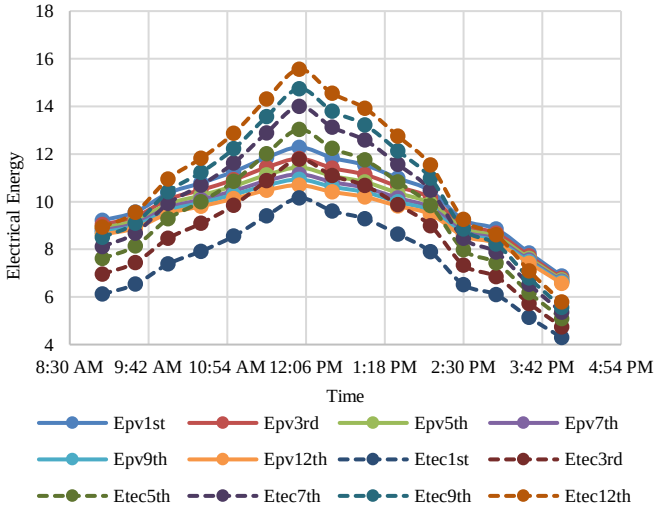

Figure 6a. Hourly variation of electrical energy from PV module ($\dot{E}_{PV,n^{th}}$), Eq. 23, and TEC ($\dot{E}_{TEC,n^{th}}$), Eq. 24, at the 1st, 3rd, 5th, 7th, 9th, and 12th PVT-TEC air collectors

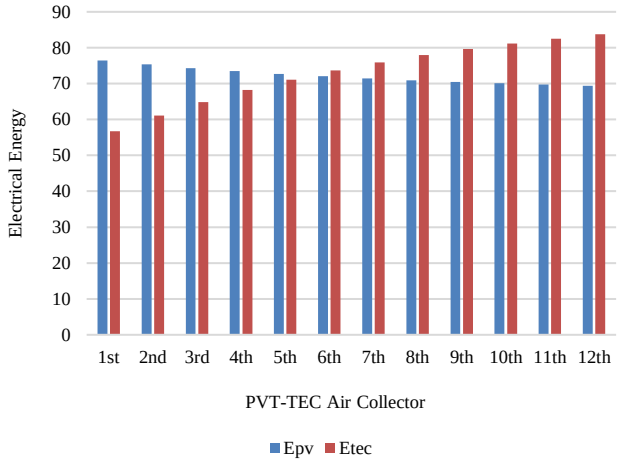

Figure 6b. Daily electrical energy from Opaque PV and TEC for different nth PV-TEC air collectors

Now, Figure 6a shows the hourly variation of electrical energy in W from PV module ($\dot{E}_{PV,n^{th}}$), Eq. 23, and electrical energy from TEC ($\dot{E}_{TEC,n^{th}}$), Eq. 24, from the 1st to 12th PVT-TEC air collectors. Figure 6b shows the daily electrical energy from PV and TEC for different nth PVT-TEC air collectors. It is noteworthy that the hourly and daily electrical energy from PV decreases with an increase in the number of nth PVT-TEC air collectors due to high thermal losses, as illustrated in Figure 5. However, the hourly and daily electrical energy from TEC increases because it depends on the difference in temperature between the top and bottom of the TEC, as shown in Figure 6. This difference increases as the number of the nth PVT-TEC increases. Therefore, in this case, the nth PVT-TEC air collector must be optimized for maximum electrical energy from PV as well as TEC. Further, one can conclude that both electrical energies from PV as well as TEC are approximately the same at the 5th PVT-TEC air collector.

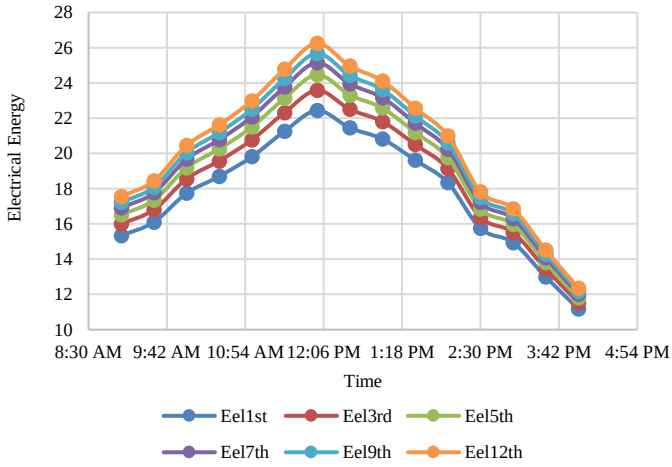

Figure 7. Hourly variation of total electrical energy($\dot{E}_{el,n^{th}}$), Eq. 23a at 1st, 3rd, 5th, 7th, 9th and 12th PVT-TEC air collector

In order to observe the hourly variation of total electrical energy in W for different nth PVT-TEC air collectors, Figure 7 is generated. It can be observed that the total electrical energy increases with an increase in the number of nth PVT-TEC air

collectors, unlike electrical energy from photo-voltaic module. In this case, increment in the total electrical energy is also reduced after the 5th PVT-TEC air collector and one can observe that the 5th PVT-TEC air collector is again optimum for given design parameters presented in Table 1. This optimization is only conducted from electrical energy point of view.

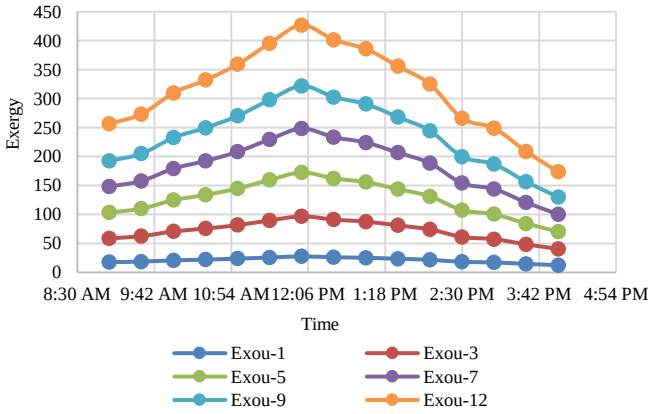

Figure 8. Hourly variation of the overall hourly thermal exergy, $\dot{E}x_{ou-N}$, Eq. 29, of N-opaque PV-TEC air collector at the 1st, 3rd, 5th, 7th, 9th, and 12th PVT-TEC air collectors

The hourly variations of the overall hourly exergy, $\dot{E}x_{ou-N}$, of the opaque PV-TEC air collector, Eq. 27, at the 1st, 3rd, 5th, 7th, 9th, and 12th PVT-TEC air collectors are shown in Figure 8. This figure illustrates that the overall exergy of the system increases with an increase in the number of nth PVT-TEC air collectors. However, the increment in the exergy becomes less significant compared to the total electrical energy, which is shown in Figure 7. Hence, the optimization of PVT air collector with respect to the overall thermal exergy is different from the earlier one, i.e., with respect to electrical energy (Figure 7).

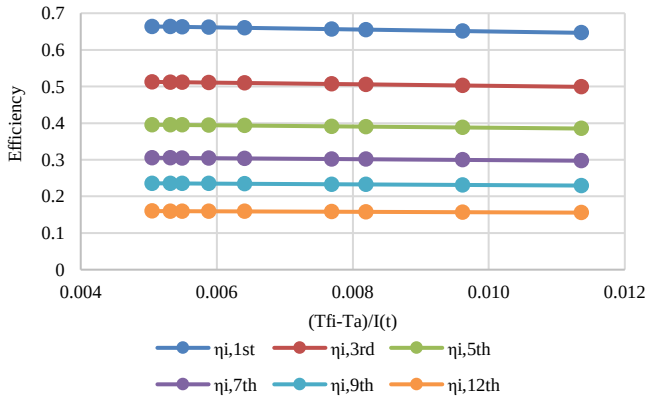

Figure 9a. Variation of instantaneous thermal efficiency $(\eta_{i,n^{th}})$ Eq. 17c with $\frac{(T_{fi}-T_a)}{I(t)}$ at the 1st, 3rd, 5th, 7th, 9th, and 12th PVT-TEC air collectors

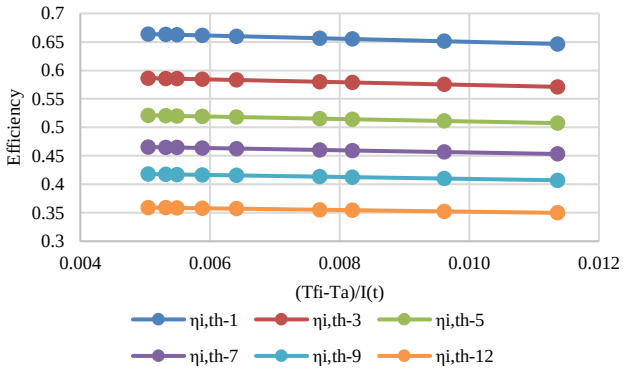

Figure 9b. Variation of instantaneous thermal efficiency $(\eta_{i,th-N})$ Eq. 27c with $\frac{(T_{fi}-T_a)}{I(t)}$ for N =1,3,5,7, 9, and 12 PVT-TEC air collectors

Figures 9a and 9b show the thermal characteristic curves for the nth and N PVT-TEC air collectors, respectively, which were drawn using Eqs. 17c and 27c. It can be observed that as n and N increase, the instantaneous thermal efficiency decreases due to an increase in operating temperature, resulting in higher thermal energy losses, as expected. It was also noted that the variation in both cases is marginal, possibly due to the considered mass flow rate of 0.003 kg/s as shown in Table 1. However, for n=N=1, the instantaneous thermal efficiency is approximately the same, but for higher values of n and N, the instantaneous efficiency is higher for the N case. This is due to the fact that the total thermal energy in this case becomes higher.

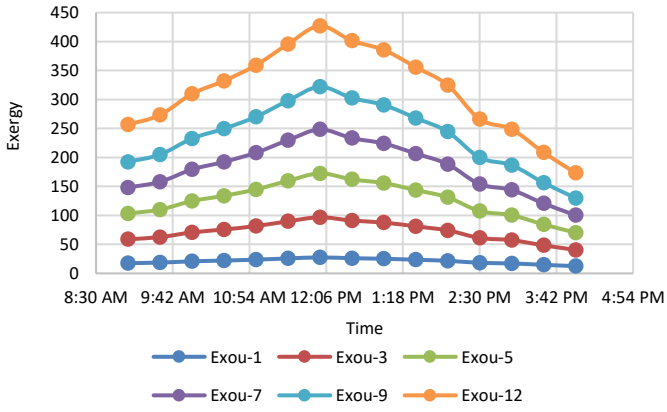

Figure 10a. Hourly variation of total exergy, Eq. 29, for N= 1.3.5.7.9, and 12

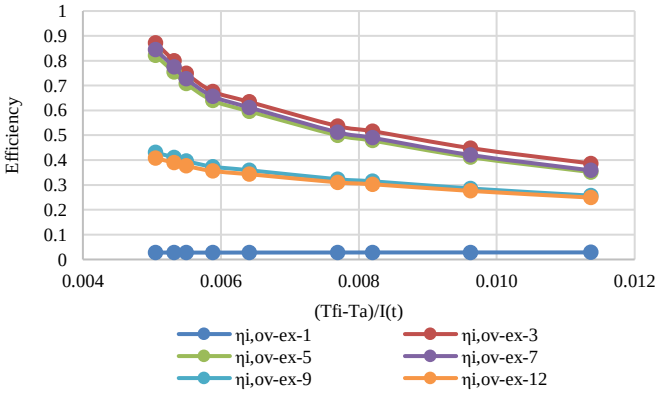

Figure 10b. Variation of the overall exergy efficiency, Eq. 30, and $\frac{(T_{fi}-T_a)}{I(t)}$.

The hourly variation of the total exergy in watts and exergy efficiency in fractions for N = 1, 3, 5, 7, 9, and 12 PVT-TEC air collectors is shown in Figure 10. It can be observed that electrical energy does not play a significant role in comparison to overall thermal exergy, as shown in Figure 7, due to its smaller value. Therefore, the exergy characteristic curve has a higher numerical value and variation in comparison to the thermal characteristic curve, as depicted in Figure 9. Furthermore, the exergy efficiency curve also increases up to the 5th PVT-TEC air collector and then begins to decrease. Hence, it can be concluded that the optimum value of n is five.

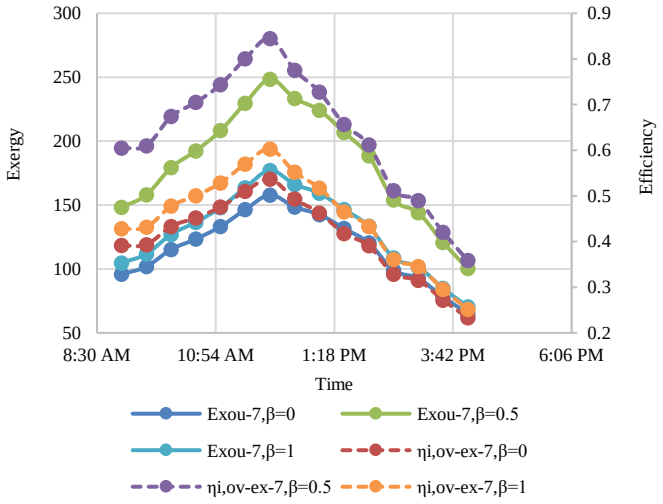

Figure 11. Effect of TEC packing factor β_{tec} (0,0.5 and 1) on the hourly variation of the total exergy (Eq. 29) and efficiency (Eq. 30) for N= 7

The effect of TEC packing factor β_{tec} on the hourly variation of total exergy for N=7 has been plotted in Figure11, considering β_tec values ranging from 0 to 1 (i.e., 0, 0.5, and 1). The results indicate that the hourly exergy is maximum for a packing factor of 0.5. Therefore, it can be concluded that the optimum value of the TEC packing factor in the case of PVT-TEC air collectors is 0.5. In this case, the temperature of the PV module and the temperature difference between the top and bottom of the TEC will determine the maximum electrical energy that can be obtained from the TEC.

6 EXPERIMENTAL VALIDATION

Equation 7 aims to ensure the experimental validation of $T_{tec,bottom}$ for the 1st PVT-TEC air collector based on the design and climatic parameters derived from the study of Dimri et. al. (Dimri et al., 2018). The hourly variation in the bottom temperature of TEC is shown in Figure 12 along with the experimental hourly variation obtained from Dimri et al. (Dimri et al., 2018). One can infer that there is reasonable agreement between theoretical results obtained by the present model and experimental value of Dimri et al. (Dimri et al., 2018). Accordingly, other hourly temperature variations can be validated by using the present model.

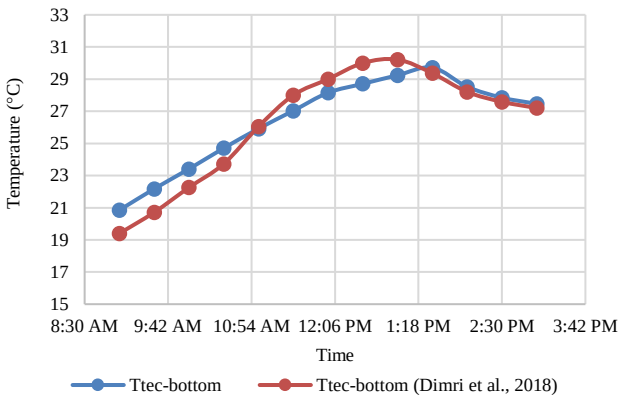

Figure 12. Comparison between the results for $T_{tec\text{-}bottom}$ and the experimental studies (Dimri et al., 2018)

7 CONCLUSIONS

Based on the present study on the N-PVT-TEC air collectors connected in series, the following conclusions were drawn:

(a) The trend in hourly variation of average solar cell temperature ($\bar{T}_{sc,n^{th}}$) and air fluid temperature changed after the 4th PVT-TEC air collector, ($\bar{T}_{f,n^{th}}$), while the trends in the top and bottom temperatures of TEC remained the same, as shown in Figure 4.
(b) The daily electrical energy from PV module decreased following an increase in the number of the nth PVT-TEC air collectors, unlike while electrical power from TEC, as shown in Figure 6b
(c) The optimum number of PVT-TEC air collectors was found to be five for the design parameters given in Table 1.
(d) The optimum packing factor of TEC was determined as 0.5 for maximum exergy and its efficiency, as given in Figure 11.

8 ACKNOWLDGEMENT

We would like to express our gratitude to Dr. M. S. Sodha for inspiring us in our research. Additionally, we extend our thanks to Dr. Neha Dimri and Dr. Arvind Tiwari for providing us with their research data, which we used to simulate our results.

APPENDIX A

The following relations are used in thermal modeling of opaque photovoltaic integrated thermoelectric cooler (PV-TEC) collector.

$$(\alpha\tau)_{eff} = \tau_g(\alpha_{sc} - \eta_{sc})$$

$$(\alpha\tau)'_{eff} = (1 - \eta_{tec})h_{p1}h_{p2}(\alpha\tau)_{eff}$$

$$U_{t,c-a} = \left[\frac{L_g}{K_g} + \frac{1}{h_o}\right]^{-1}$$

$$h_o = 5.7 + 3.8V$$

$$h_t = \frac{K_t}{L_t}$$

$$U_{b,c-a} = \left[\frac{L_t}{K_t} + \frac{1}{h_i}\right]^{-1}$$

$$h_i = 2.8 + 3V; V = 1m/s$$

$$h_{p1} = \frac{h_t\beta_{tec}}{U_{t,c-a} + U_{b,c-a}(1-\beta_{tec}) + h_t\beta_{tec}}$$

$$U_{tec,top-a} = \frac{h_t\beta_{tec}U_{t,c-a}}{U_{t,c-a} + U_{b,c-a}(1-\beta_{tec}) + h_t\beta_{tec}}$$

$$U_{tec,top-f} = \frac{h_t\beta_{tec}U_{b,c-a}(1-\beta_{tec})}{U_{t,c-a} + U_{b,c-a}(1-\beta_{tec}) + h_t\beta_{tec}}$$

$$h_{p2} = \frac{U_{tec}\beta_{tec}}{U_{tec,top-a} + U_{tec,top-f} + U_{tec}\beta_{tec}}$$

$$U_{tec,bottom-a} = \frac{U_{tec}\beta_{tec}U_{tec,top-a}}{U_{tec,top-a} + U_{tec,top-f} + U_{tec}\beta_{tec}}$$

$$U_{tec,bottom-f} = \frac{U_{tec}\beta_{tec}U_{tec,top-f}}{U_{tec,top-a} + U_{tec,top-f} + U_{tec}\beta_{tec}}$$

The heat transfer coefficient from the bottom-end of TEC module to fluid (h_{tf}) flowing below it, considering laminar flow, is calculated as:

$$h_{tf} = \frac{K_f}{L}Nu = \frac{K_f}{L} \times (0.332)Re^{\frac{1}{2}}Pr^{\frac{1}{3}}$$
$$= \frac{0.02622}{0.37} \times (0.332)$$
$$\times (1.10846 \times 10^4)^{\frac{1}{2}}0.708^{\frac{1}{3}} = 2.21W/m^2K$$

where Nu is Nusselt number, Pr is Prandtl number, and Re is Reynold number. Reynold number (Re) is obtained as follows:

$$Re = \frac{VL}{\nu} = \frac{\dot{m}_f L}{bL_f\rho\nu} = \frac{0.003 \times 0.37}{0.36 \times 0.01 \times 1.774 \times (15.68 \times 10^{-6})}$$
$$= 1.10846 \times 10^4$$

The constants used in Eqs. are defined as:

$$U_b = \left[\frac{L_i}{K_i} + \frac{1}{h_i}\right]^{-1}$$

$$U_{fa} = U_{fa,1} + U_{fa,2} + U_{fa,3} + U_{fa,4}$$

$$U_{fa,1} = \frac{h_{tf}\beta_{tec}(1-\eta_{tec})U_{tec,bottom-a}}{h_{tf}\beta_{tec} + (1-\eta_{tec})U_{tec,bottom-a} + (1-\eta_{tec})U_{tec,bottom-f}}$$

$$U_{fa,2} = \frac{U_{t,c-a}U_{b,c-a}(1-\beta_{tec})}{U_{t,c-a} + U_{b,c-a}(1-\beta_{tec}) + h_t\beta_{tec}}$$

$$U_{fa,3} = \frac{h_t\beta_{tec}U_{b,c-a}(1-\beta_{tec})U_{tec,top-a}}{\left[U_{t,c-a} + U_{b,c-a}(1-\beta_{tec}) + h_t\beta_{tec}\right]\left[U_{tec,top-a} + U_{tec,top-f} + U_{tec}\beta_{tec}\right]}$$

$$U_{fa,4} = \frac{h_t\beta_{tec}U_{b,c-a}(1-\beta_{tec})U_{tec}\beta_{tec}(1-\eta_{tec})U_{tec,bottom-a}}{\left[U_{t,c-a} + U_{b,c-a}(1-\beta_{tec}) + h_t\beta_{tec}\right]\left[U_{tec,top-a} + U_{tec,top-f} + U_{tec}\beta_{tec}\right]\left[h_{tf}\beta_{tec} + (1-\eta_{tec})U_{tec,bottom-a} + (1-\eta_{tec})U_{tec,bottom-f}\right]}$$

$$h_{p3} = \frac{h_{tf}\beta_{tec}}{h_{tf}\beta_{tec} + (1-\eta_{tec})U_{tec,bottom-a} + (1-\eta_{tec})U_{tec,bottom-f}}$$

$$h'_{p1} = \frac{U_{b,c-a}(1-\beta_{tec})}{U_{t,c-a} + U_{b,c-a}(1-\beta_{tec}) + h_t\beta_{tec}}$$

$$h'_{p2} = \frac{h_t\beta_{tec}U_{b,c-a}(1-\beta_{tec})}{\left[U_{t,c-a} + U_{b,c-a}(1-\beta_{tec}) + h_t\beta_{tec}\right]\left[U_{tec,top-a} + U_{tec,top-f} + U_{tec}\beta_{tec}\right]}$$

$$h'_{p3} = \frac{h_t\beta_{tec}U_{b,c-a}(1-\beta_{tec})U_{tec}\beta_{tec}}{\left[U_{t,c-a} + U_{b,c-a}(1-\beta_{tec}) + h_t\beta_{tec}\right]\left[U_{tec,top-a} + U_{tec,top-f} + U_{tec}\beta_{tec}\right]\left[h_{tf}\beta_{tec} + (1-\eta_{tec})U_{tec,bottom-a} + (1-\eta_{tec})U_{tec,bottom-f}\right]}$$

NOMENCLATURE

A_m	Aea of module (m^2)
L	Length of collector (m)
b	Breadth of collector (m)
c_f	Specific heat of fluid (J/kgK)
dx	Elemental length (m)
I(t)	Global solar radiation (W/m^2)
$\dot{m}$	Mass flow rate of fluid (kg/s)
K_g	Thermal conductivity of glass (W/mK)
K_t	Thermal conductivity of tedlar (W/mK)
K_{tec}	Thermal conductivity of TEC module (W/mK)
K_i	Thermal conductivity of insulation (W/mK)
K_f	Thermal conductivity of fluid/air (W/mK)
L_g	Thickness of glass cover (m)
L_t	Thickness of tedlar (m)
L_{tec}	Thickness of TEC module (m)
L_i	Thickness of insulation (m)
L_f	Thickness of fluid/air column in the duct (m)
h_t	heat transfer coefficient from back of solar cells to the top end of TEC module (W/m^2K)
h_{tf}	Heat transfer coefficient from the bottom-end of TEC module to fluid (W/m^2K)
$U_{t,c-a}$	Overall heat transfer coefficient from top of solar cells to ambient through glass cover (W/m^2K)
U_b	Overall heat transfer coefficient from bottom of insulation to ambient (W/m^2K)
$U_{tec,top-a}$	Overall heat transfer coefficient from top-end of TEC module to ambient (W/m^2K)
$U_{tec,bottom-a}$	Overall heat transfer coefficient from bottom-end of TEC module to ambient (W/m^2K)
$U_{tec,top-f}$	Overall heat transfer coefficient from top-end of TEC module to fluid (W/m^2K)

$U_{tec,bottom-f}$	Overall heat transfer coefficient from bottom-end of TEC module to fluid (W/m^{2}K)
U_{fa}	Overall heat transfer coefficient from fluid to ambient (W/m^{2}K)
$U_{b,c-a}$	Overall heat transfer coefficient from bottom of solar cells to ambient through tedlar (W/m^{2}K)
h_{p1}	First penalty factor due to glass cover
h_{p2}	Second penalty factor due to tedlar
h_{p3}	Third penalty factor due to TEC module
η_o	Solar cell efficiency at standard test condition, i.e. I(t)=1000 W/m^2 and To=25°C
η_{tec}	Conversion efficiency from thermal energy to electricalenergy of TEC module
β_o	Temperature coefficient of solar cell efficiency (K−1)

Greek letters

α	Absorptivity
β	Packing factor
τ	Transmittivity
η	Efficiency
$(\alpha\tau)_{eff}$	Product of effective absorptivity and transmittivity

Subscripts

a	Ambient
eff	Effective
f	Fluid
fi	Fluid inlet
fo	Fluid outlet
g	Glass
m	Module
sc	Solar cell
tec	TEC module
t	Tedlar
i	Insulation

REFERENCES

1. Arslan, E., Aktaş, M., & Can, Ö. F. (2020). Experimental and numerical investigation of a novel photovoltaic thermal (PV/T) collector with the energy and exergy analysis. *Journal of Cleaner Production*, *276*, 123255. https://doi.org/10.1016/j.jclepro.2020.123255
2. Atheaya, D., Tiwari, A., & Tiwari, G. N. (2016). Exergy analysis of photovoltaic thermal (PVT) compound parabolic concentrator (CPC) for constant collection temperature mode. *Solar Energy*, *135*, 222–231. https://doi.org/10.1016/j.solener.2016.05.055
3. Badiei, Z., Eslami, M., & Jafarpur, K. (2020). Performance improvements in solar flat plate collectors by integrating with phase change materials and fins: A CFD modeling. *Energy*, *192*. https://doi.org/10.1016/j.energy.2019.116719
4. Bejan, A. (1978). General criterion for rating heat-exchanger performance. *International Journal of Heat and Mass Transfer*, *21*(5), 655–658. https://doi.org/10.1016/0017-9310(78)90064-9
5. Cabral, D., Gomes, J., & Karlsson, B. (2019). Performance evaluation of non-uniform illumination on a transverse bifacial PVT receiver in combination with a CPC geometry. *Solar Energy*, *194*, 696–708. https://doi.org/10.1016/j.solener.2019.10.069
6. Cengel, Y. A., & Boles, M. A. (2015). *Thermodynamics: An Engineering Approach*. McGraw- Hill Education, New York. https://www.mheducation.com/highered/product/thermodynamics-engineering-approach-cengel-boles/M9781259822674.html
7. Chow, T. T. (2010). A review on photovoltaic / thermal hybrid solar technology. *Applied Energy*, *87*(2), 365–379. https://doi.org/10.1016/j.apenergy.2009.06.037
8. Dimri, N., Tiwari, A., & Tiwari, G. N. (2018). Effect of thermoelectric cooler (TEC) integrated at the base of opaque photovoltaic (PV) module to enhance an overall electrical efficiency. *Solar Energy*, *166*(November 2017), 159–170. https://doi.org/10.1016/j.solener.2018.03.030
9. Dincer, I. (2002). The role of exergy in energy policy making. *Energy Policy*, *30*(2), 137–149. https://doi.org/10.1016/S0301-4215(01)00079-9
10. Dincer, I., & Rosen, M. A. (2013). Chapter 2 - Exergy and Energy Analyses. In I. Dincer & M. A. Rosen (Eds.), *Exergy (Second Edition)* (Second Edition, pp. 21–30). Elsevier. https://doi.org/10.1016/B978-0-08-097089-9.00002-4
11. Dubey, S., & Tiwari, G. N. (2008). *Thermal modeling of a combined system of photovoltaic thermal (PV / T) solar water heater*. *82*, 602–612. https://doi.org/10.1016/j.solener.2008.02.005
12. Duffie, J. A., & Beckman W. A. (2013). *Solar Engineering of Thermal Processes*. John Wiley & Sons, Inc. https://doi.org/10.1002/9781118671603
13. Dupeyrat, P., Ménézo, C., & Fortuin, S. (2014). Study of the thermal and electrical performances of PVT solar hot water system. *Energy and Buildings*, *68*, 751–755. https://doi.org/10.1016/j.enbuild.2012.09.032
14. Evans, D. L. (1981). Simplified method for predicting photovoltaic array output. *Solar Energy*, *27*(6), 555–560. https://doi.org/10.1016/0038-092X(81)90051-7
15. Hocine, H. B. C. El, Touafek, K., Kerrour, F., Haloui, H., & Khelifa, A. (2015). Model Validation of an Empirical Photovoltaic Thermal (PV/T) Collector. *Energy Procedia*, *74*, 1090–1099. https://doi.org/10.1016/J.EGYPRO.2015.07.749
16. Hoseinzadeh, S., Ghasemi, M. H., & Heyns, S. (2020). Application of hybrid systems in solution of low power generation at hot seasons for micro hydro systems. *Renewable Energy*, *160*, 323–332. https://doi.org/10.1016/j.renene.2020.06.149
17. Hoseinzadeh, S., & Heyns, P. S. (2020). Advanced Energy, Exergy, and Environmental (3E) Analyses and Optimization of a Coal-Fired 400 MW Thermal Power Plant. *J. Energy Resour. Technol.*, *143*(8), 082106 (9 pages). https://doi.org/10.1115/1.4048982
18. Hoseinzadeh, S., Yargholi, R., Kariman, H., & Heyns, P. S. (2020). Exergoeconomic analysis and optimization of reverse osmosis desalination integrated with geothermal energy. *Environmental Progress and Sustainable Energy*, *39*(5). https://doi.org/10.1002/ep.13405
19. Huen, P., & Daoud, W. A. (2017). Advances in hybrid solar photovoltaic and thermoelectric generators. *Renewable and Sustainable Energy Reviews*, *72*(October), 1295–1302. https://doi.org/10.1016/j.rser.2016.10.042
20. Jafari, S., Sohani, A., Hoseinzadeh, S., & Pourfayaz, F. (2022). The 3E Optimal Location Assessment of Flat-Plate Solar Collectors for Domestic Applications in Iran. *Energies*, *15*(10), 1–17. https://doi.org/10.3390/en15103589
21. Kariman, H., Hoseinzadeh, S., & Heyns, P. S. (2019). Energetic and exergetic analysis of evaporation desalination system integrated with mechanical vapor recompression circulation. *Case Studies in Thermal Engineering*, *16*, 100548. https://doi.org/10.1016/J.CSITE.2019.100548
22. Kariman, H., Hoseinzadeh, S., Heyns, S., & Sohani, A. (2020). Modeling and exergy analysis of domestic med desalination with brine tank. *Desalination and Water Treatment*, *197*, 1–13. https://doi.org/10.5004/dwt.2020.26105
23. Kostić, L. T., Pavlović, T. M., & Pavlović, Z. T. (2010). Optimal design of orientation of PV/T collector with reflectors. *Applied Energy*, *87*(10), 3023–3029. https://doi.org/10.1016/j.apenergy.2010.02.015
24. Kotb, A., Elsheniti, M. B., & Elsamni, O. A. (2019). Optimum number and arrangement of evacuated-tube solar collectors under various operating conditions. *Energy Conversion and Management*, *199*(September), 112032. https://doi.org/10.1016/j.enconman.2019.112032
25. Li, M., Zhong, D., Ma, T., Kazemian, A., & Gu, W. (2020). Photovoltaic thermal module and solar thermal collector connected in series: Energy and exergy analysis. *Energy Conversion and Management*, *206*(November 2019), 112479. https://doi.org/10.1016/j.enconman.2020.112479
26. Ma, T., Li, M., & Kazemian, A. (2020). Photovoltaic thermal module and solar thermal collector connected in series to produce electricity and high-grade heat simultaneously. *Applied Energy*, *261*(October 2019), 114380. https://doi.org/10.1016/j.apenergy.2019.114380
27. Ong, K. S., Naghavi, M. S., & Lim, C. (2017). Thermal and electrical performance of a hybrid design of a solar-thermoelectric system. *Energy Conversion and Management*, *133*, 31–40. https://doi.org/10.1016/j.enconman.2016.11.052
28. Ouyang, Z., & Li, D. (2016). Modelling of segmented high-performance thermoelectric generators with effects of thermal radiation, electrical and thermal contact resistances. *Scientific Reports*, *6*(April), 1–12. https://doi.org/10.1038/srep24123

29. Proell, M., Osgyan, P., Karrer, H., & Brabec, C. J. (2017). Experimental efficiency of a low concentrating CPC PVT flat plate collector. *Solar Energy*, *147*, 463–469. https://doi.org/10.1016/j.solener.2017.03.055

30. Sarwar, J., Khan, M. R., Rehan, M., Asim, M., & Kazim, A. H. (2020). Performance analysis of a flat plate collector to achieve a fixed outlet temperature under semi-arid climatic conditions. *Solar Energy*, *207*(April), 503–516. https://doi.org/10.1016/j.solener.2020.06.088

31. Sharaf, O. Z., & Orhan, M. F. (2018). Comparative thermodynamic analysis of densely-packed concentrated photovoltaic thermal (CPVT) solar collectors in thermally in-series and in-parallel receiver configurations. *Renewable Energy*, *126*, 296–321. https://doi.org/10.1016/j.renene.2018.03.026

32. Shyam, Tiwari, G. N., Fischer, O., Mishra, R. K., & Al-Helal, I. M. (2016). Performance evaluation of N -photovoltaic thermal (PVT) water collectors partially covered by photovoltaic module connected in series: An experimental study. *Solar Energy*, *134*, 302–313. https://doi.org/10.1016/j.solener.2016.05.013

33. Skoplaki, E., & Palyvos, J. A. (2009). On the temperature dependence of photovoltaic module electrical performance: A review of efficiency/power correlations. *Solar Energy*, *83*(5), 614–624. https://doi.org/10.1016/j.solener.2008.10.008

34. Sudharshan, K. Y., Kumar, V. P., & Barshilia, H. C. (2016). Performance evaluation of a thermally concentrated solar thermo-electric generator without optical concentration. *Solar Energy Materials and Solar Cells*, *157*, 93–100. https://doi.org/10.1016/j.solmat.2016.05.033

35. Tiwari, G. N., & Dubey S. (2010). Fundamentals of Photovoltaic Modules and Their Applications. *Royal Society of Chemistry (RSC), (UK)*. https://link.springer.com/book/9781849730204

36. Tiwari, G. N., Meraj, M., & Khan, M. E. (2018). Exergy analysis of N-photovoltaic thermal-compound parabolic concentrator (N-PVT-CPC) collector for constant collection temperature for vapor absorption refrigeration (VAR) system. *Solar Energy*, *173*, 1032–1042. https://doi.org/10.1016/j.solener.2018.08.031

37. Tiwari, G. N., Tiwari, A., & Shayam. (2016). *Handbook of solar energy*. Springer. https://doi.org/10.1007/978-981-10-0807-8

38. Vega, J., & Cuevas, C. (2020). Parallel vs series configurations in combined solar and heat pump systems: A control system analysis. *Applied Thermal Engineering*, *166*, 114650. https://doi.org/10.1016/j.applthermaleng.2019.114650

39. Yin, E., Li, Q., & Xuan, Y. (2017). Thermal resistance analysis and optimization of photovoltaic-thermoelectric hybrid system. *Energy Conversion and Management*, *143*, 188–202. https://doi.org/10.1016/j.enconman.2017.04.004

40. Zhang, J., Xuan, Y., & Yang, L. (2014). Performance estimation of photovoltaic-thermoelectric hybrid systems. *Energy*, *78*, 895–903. https://doi.org/10.1016/j.energy.2014.10.087

41. Zhu, W., Deng, Y., Wang, Y., Shen, S., & Gulfam, R. (2016). High-performance photovoltaic-thermoelectric hybrid power generation system with optimized thermal management. *Energy*, *100*, 91–101. https://doi.org/10.1016/j.energy.2016.01.055

42. Zondag, H. A., de Vries, D. W., van Helden, W. G. J., van Zolingen, R. J. C., & van Steenhoven, A. A. (2003). The yield of different combined PV-thermal collector designs. *Solar Energy*, *74*(3), 253–269. https://doi.org/10.1016/S0038-092X(03)00121-X